A LARGE EDDY SIMULATION OF HURRICANE INTENSIFICATION

81

Stephen R. Guimond[1*], Sydney Sroka[2] and Devin Protzko[3]

[1]*University of Maryland Baltimore County/JCET, Baltimore, MD*
[2]*Massachusetts Institute of Technology Lorenz Center, Cambridge, MA*
[3]*University of Maryland Baltimore County, Baltimore, MD*

1. INTRODUCTION

The range of spatial and temporal scales controlling the dynamics of geophysical fluid flows are vast and span several orders of magnitude from large-scale Rossby waves in the atmosphere (~ 10,000 km) to small-scale eddies responsible for viscous dissipation in the atmosphere and ocean (~ millimeters). This wide range of scales, and particularly the nonlinear interactions between them, pose significant difficulties for observational systems and numerical simulations. An excellent example of a geophysical phenomenon possessing these characteristics is the hurricane. Figure 1 shows the kinetic energy density of physical processes controlling hurricane intensification as a function of wavelength. Errors in the specification of convective cloud properties, such as the latent heating rate, can propagate up to the vortex scale affecting the prediction and understanding of the intensification process. Recently, it has also been demonstrated that differences in the implicit diffusion characteristics of atmospheric dynamic cores can affect the system scale dynamics of hurricanes by affecting the nonlinear energy transfer (Guimond et al. 2016).

While the importance of the turbulent scales of motion (defined here as wavelengths of ~ 1 km and below) in geophysical and computational fluid dynamics has been known for many years (e.g. Tennekes and Lumley 1972; Stull 1988; Grinstein et al. 2007), the study of turbulence in hurricanes is a fairly young field (e.g. Zhang et al. 2009; Rotunno et al. 2009; Bryan et al. 2010; Nakanishi and Niino 2012; Guimond et al. 2018). The primary reasons for this are the lack of dense volumes of high-resolution observations that can probe deep into the boundary layer, the region of most significant turbulence, and computer resource limitations that inhibit the explicit calculation of turbulent eddies in the full hurricane domain. The circulation of hurricanes can extend out to 500 km radius or more; consequently, using a square model domain of 1000 km on a side with a grid spacing of 0.1 mm (Kolmogorov microscale) would require 10^{20} grid points for one level of calculation, not to mention the very small time step required for numerical stability. Fortunately, it may not be necessary to resolve a simulation down to the smallest dissipative eddies and static or adaptive mesh refinement techniques can reduce the overall size of the simulation while still capturing the most critical portions of the flow with high resolution.

On the measurement side, new airborne Doppler radars are capable of sampling deep into the hurricane boundary layer allowing three-dimensional wind retrievals with ~ 200 m horizontal and 30 m vertical grid spacing (Guimond et al. 2014; Guimond et al. 2018). These measurements are beginning to provide a unique examination of coherent turbulence in intense hurricanes and its role in intensity change, which should provide the community with critical data for various applications. *The purpose of this work is to present new results from a large eddy simulation (LES) of an idealized hurricane at 60 m grid spacing and use the resulting data to understand the sampling characteristics of new airborne Doppler radars. In addition, the role of asymmetric dynamics in the intensification process is analyzed using angular momentum budgets with the model output.*

2. NUMERICAL SIMULATIONS

In order to provide data to study the sampling and wind retrieval characteristics of new airborne Doppler radars, a numerical simulation that explicitly resolves large turbulent eddies was conducted. The High Gradient (HIGRAD) model, which solves the compressible, nonhydrostatic Navier-Stokes equations with a finite volume and semi-implicit dynamic core (Reisner et al. 2005; Guimond et al. 2016) was used to simulate the hurricane intensification process. Guimond et al. (2016) showed that the HIGRAD dynamic core has a minimal amount of numerical diffusion when compared to community cores such as the Weather

* *Corresponding author address:* Stephen R. Guimond, Univ. of Maryland, Baltimore County, Dept. of Physics, Baltimore, MD 21250; e-mail: sguimond@umbc.edu

Research and Forecasting (WRF) model. For idealized simulations, the vortex response to asymmetric heating perturbations was significantly damped in WRF relative to HIGRAD as well as a spectral element core, which affected the system scale intensity by muting the nonlinear, upscale transfer of energy.

The current HIGRAD simulations were modeled after the rapid intensification of Hurricane Guillermo (1997) with an initial vortex in thermal wind balance and maximum wind speed of ~ 20 m s^{-1} at a radius of maximum wind (RMW) of ~ 35 km (see Guimond et al. 2016 for more details). This initial vortex is similar to Guillermo with the exception of a weaker maximum wind speed and dynamically stable, balanced state. The model domain is a square with a length of ~ 600 km on a side and constant horizontal grid spacing of 60 m in a patch centered on the vortex with a length of 40 km on each side. An exponential function is used to smoothly transition from the edge of the patch to a grid spacing of 5 km on the domain edges.

Figure 2 shows a radial profile of the initial, axisymmetric tangential velocity at the lowest model level along with the associated grid spacing. The inner core of the vortex (radius < 50 km) is covered with a horizontal grid spacing of 60 – 75 m. The vertical grid uses 210 stretched levels with 60 – 75 m spacing up to ~ 7 km height and ~ 150 m spacing near the model top of 18 km. A 3 km deep Rayleigh absorbing layer is included at the model top to dissipate upward propagating energy from inertia-gravity waves. The simulations are dry, but the vortex is perturbed with four-dimensional distributions of latent heating calculated from airborne Doppler radar observations during the rapid intensification of Guillermo (Guimond et al. 2011; Guimond et al. 2012). Figure 3 shows three-dimensional isosurfaces of the latent heating and cooling retrievals in Guillermo along with the time evolution function used to merge the data into the model. Details can be found in Guimond et al. (2012). No surface dissipation is included at the lower boundary to focus specifically on the vortex response to heating. Exclusion of surface dissipation is not expected to make a significant impact on the goals of this study because the simulations produce a reasonably realistic turbulent field that can be used to understand new radar measurements and the basic vortex dynamics.

The implied filtering of the governing equations that results when choosing a grid spacing larger than the scale of the smallest dissipative eddies (Kolmogorov microscale) results in a term that involves the divergence of the stress tensor (τ_{ij}),

$$\frac{\partial u_i}{\partial t} + \frac{\partial u_i u_j}{\partial x_j} = RHS - \frac{\partial \tau_{ij}}{\partial x_j}, \qquad (1)$$

where u_i is the three-dimensional velocity and RHS represents the standard terms on the right-hand-side of the Navier-Stokes equations written in summation notation. Neglecting the viscous shear component of the stress and assuming a first order turbulence closure (Stull 1988), the stress tensor can be approximated as

$$\tau_{ij} = -\kappa \frac{\partial u_i}{\partial x_j}, \qquad (2)$$

where κ is the sub-grid scale diffusion coefficient. For the LES described in this study, constant coefficients of 200 m^2 s^{-1} in the horizontal and vertical dimensions are used. Inserting (2) back into (1) yields a Laplacian diffusion operator

$$\frac{\partial u_i}{\partial t} + \frac{\partial u_i u_j}{\partial x_j} = RHS + \kappa \frac{\partial^2 u_i}{\partial x_j^2}. \qquad (3)$$

Note that we also use a Laplacian diffusion term on the RHS of the energy (potential temperature) equation. At the 60 m grid spacing used here, the large eddies in the flow that provide the bulk of the turbulent flux of energy and momentum are explicitly resolved. The sub-grid scale motions, which are intended to represent the small, dissipative eddies in the flow, are parameterized through the Laplacian diffusion term.

Despite the use of a stretched mesh, the simulations take a large amount of computer time since the time step needed for stability was ~ 1.5×10^{-1} s. Figure 4 shows a snapshot of the horizontal wind speed at ~ 5 km height and 2.5 h into the simulation revealing small-scale eddies present in the eyewall of the vortex as well as turbulent mixing between the eye and eyewall. Note that the vortex drifts slowly southeast over time due to a wavenumber one asymmetry implicit in the latent heat forcing.

Although the numerical simulations are idealized, we want the large turbulent eddies explicitly resolved by the model to represent a reasonable characterization of turbulence in a real hurricane. To examine this, we have compared turbulence statistics from 1 Hz flight level data in Hurricane Guillermo (1997) to those computed from the numerical simulation. Flight level data at ~ 3 km height from four radial penetrations through the center of Guillermo was interpolated to a radial grid with spacing of 180 m. Data from the numerical simulation was generated in the same fashion and interpolated to the same radial grid. Two statistics were analyzed for the comparisons: the turbulent kinetic energy (TKE) per unit mass, $TKE = 1/2((u')^2 + (v')^2 + (w')^2)$, and the TKE spectrum per unit mass, $E(k) = 0.5(\widehat{u'^2} + \widehat{v'^2})$. The perturbation variables (denoted by primes) are defined by subtracting out the mean wind component for each radial leg from the total. The variables with a hat denote the de-trended discrete Fourier transformed fields. The energy spectrum is a function of the wavenumber (*k*) or wavelength.

Figure 5a shows histograms of the TKE from the flight level observations and the LES. Both histograms reveal an approximately log-normal distribution with the observations and simulation showing a larger number of small and medium values, respectively. Good agreement is found at larger values of TKE (> 150 m^2 s^{-2}) located in the eyewall and at the eye-eyewall interface. Figure 5b shows the mean TKE spectrum computed over the four radial legs for both the observations and simulation. While the simulation shows more energy present at nearly all scales, the slope of the energy spectrum is very similar to the observations and the Kolmogorov theory of -5/3. The larger energy in the simulation could be due to several things such as a different initial vortex, errors in the latent heat forcing and not enough dissipation in the sub-grid model. The statistical results in Fig. 5 indicate that the LES is producing a reasonably accurate depiction of turbulence in a real, intensifying hurricane and are suitable for the goals of the paper. In general, the turbulence intensity and energy in the large eddy scales is a bit too high relative to the flight level data. Improvements to the simulations in terms of a more accurate sub-grid model that adds dynamic dissipation may be necessary.

3. SIMULATED OBSERVATIONS

The Imaging Wind and Rain Airborne Profiler (IWRAP) is a downward-pointing, conically scanning, dual-frequency, Doppler radar that measures surface backscatter, volume reflectivity and Doppler velocity at 30 m range resolution with a scan rate of 60 rpm (revolutions per minute; Fernandez et al. 2005). The IWRAP radar has been flying through hurricanes on the NOAA WP-3D aircraft for many years with a focus on ocean surface scattering signatures of high wind regions. Recently, algorithms and data analysis procedures have been designed to process the volume echo into three-dimensional Cartesian velocities with horizontal and vertical grid spacing of ~ 200 m and 30 m, respectively (Guimond et al. 2014; Guimond et al. 2018). This new data processing allows an examination of the full IWRAP database that extends from current operations back to 2003, which includes sampling of many category 4 and 5 storms.

A useful step towards understanding these measurements is an analysis of the structures and scales of motion that can be captured by new airborne radars such as IWRAP. To this end, simulated Doppler velocity observations from IWRAP were computed using the model output,

$$V_r = (ux + vy + wz)r^{-1} \tag{4}$$

where *u,v* and *w* are the Cartesian velocities interpolated to the Earth-relative radar coordinates (*x,y* and *z*) given in Guimond et al. (2014) and Guimond et al. (2018) and *r* is the range. A typical radial flight pattern through the model simulated eyewall was constructed and IWRAP wind retrievals with 250 m grid spacing (Δx) in both the horizontal and vertical directions were computed. The effective resolution of the 3D wind retrievals is dictated by the grid spacing of the analysis, footprint of the radar beam and damping characteristics of the solution method. The instrument beamwidth is neglected in the estimate of the effective resolution of the IWRAP wind retrievals because the footprint is only ~ 200 m at the surface, which is at or below the filtering scale of the retrieval grid (Guimond et al. 2018).

Figure 6a shows vertical cross sections of horizontal wind speed at nadir for the simulated truth field on the native model grid revealing a rich spectrum of eddies present in the eyewall region (~ 12 – 30 km along track) and intense, localized wind speed values greater than 60 m s^{-1}. Some of the high momentum air from the eyewall has been mixed into the eye region (~ 0 – 10 km along track). The simulated IWRAP wind retrievals in Fig. 6b indicate that the bulk of the large-scale turbulent eddies in the eye and eyewall regions are being captured, but clearly the details of the eddies are not resolved. To quantify the resolved scales in the IWRAP wind retrievals, spectral analysis is performed on the data. Figure 7 shows the kinetic energy spectrum for the model simulated truth and IWRAP wind retrievals averaged over the radar sampling volume with two main features of interest. First, the model simulated kinetic energy spectrum displays an inertial subrange, matching well with the -5/3 slope from turbulence theory. Second, the IWRAP spectrum begins to display damped energy behavior relative to the simulated spectrum and theoretical slope at wavelengths slightly larger than 1 km. This means that scales of ~ 1 km and larger (4 – 5 Δx) are nearly fully resolved by the IWRAP wind retrievals, which are capable of characterizing large, turbulent eddies in the flow. For example, Zhang et al. (2011) analyzed 40 Hz flight-level data in the boundary layer of intense hurricanes and found that the horizontal length scales of the large, dominant eddies are ~ 500 – 3000 m with a vertical scale of ~ 100 m.

4. THE ROLE OF ASYMMETRIC DYNAMICS

The intensification of hurricanes is driven by axisymmetric and asymmetric processes to varying degrees. While axisymmetric or mean dynamics typically plays the largest role, the influence of asymmetric or eddy dynamics is still being investigated with some studies omitting these effects (e.g. Emanuel 1986) or finding a negligible role (e.g. Nolan and Grasso 2003) while others have found significant impacts (e.g. Montgomery et al. 2006; Persing et al. 2013; Guimond et al. 2016). The role of asymmetric dynamics is investigated here using the LES, which is a quasi-idealized representation of the intensification of Hurricane Guillermo (1997). Absolute angular momentum (AAM) budgets are performed on the LES and compared to simulations performed at 2 km horizontal and 250 m vertical grid spacing (hereafter called "coarse"), which is a common resolution used for understanding hurricane dynamics (e.g. Persing et al. 2013). The axisymmetric AAM budget equation can be expressed as

$$\frac{\partial \overline{M_a}}{\partial t} = -\frac{1}{\bar{\rho} r}\frac{\partial(r\bar{\rho}\bar{u}\overline{M_a})}{\partial r} - \frac{1}{\bar{\rho}}\frac{\partial(\bar{\rho}\bar{w}\overline{M_a})}{\partial z} - \frac{1}{\bar{\rho} r}\frac{\partial\left(r\bar{\rho}\overline{u'M_a'}\right)}{\partial r} - \frac{1}{\bar{\rho}}\frac{\partial\left(\bar{\rho}\overline{w'M_a'}\right)}{\partial z} + \bar{D} \quad (5)$$

where $M_a = rv + 1/2f_o r^2$ is the AAM, r is the radius, u, v and w are the radial, tangential and vertical velocity, respectively, f_o is the constant Coriolis frequency (5.0×10^{-5} s^{-1}) and ρ is the density. The overbar and primes denote azimuthal mean and eddy terms, respectively. The $\bar{D}$ term represents sub-grid scale diffusion and takes the form

$$\bar{D} = \kappa\nabla^2\overline{M_a} = \kappa\left(\frac{\partial^2\overline{M_a}}{\partial r^2} + \frac{1}{r}\frac{\partial\overline{M_a}}{\partial r} + \frac{\partial^2\overline{M_a}}{\partial z^2}\right). \quad (6)$$

To focus on the impacts of the resolved dynamics in the intensification process, the strength of the sub-grid diffusion in (3) and (5) should adjust in the large eddy and coarse resolution simulations as a result of the differences in scale. If the diffusion coefficient chosen for the LES (200 m^2 s^{-1}) is used in the coarse simulation, then the vortex becomes more intense because energy dissipation isn't an active player in the budget due to the discretization coefficient, $\left(\frac{\Delta t}{\Delta x^2}, \frac{\Delta t}{\Delta z^2}\right)$. In order for the diffusion terms to play the same role in the coarse simulation, the coefficient must be set to ~ 20,000 m^2 s^{-1} in the horizontal and 400 m^2 s^{-1} in the vertical. To examine this effect, two coarse simulations were run: one with the larger diffusion coefficient values and one with the same values as the LES.

Figure 8a shows the maximum horizontal wind speed for the LES and the two coarse simulations. After approximately 1 h, the maximum wind speed in the LES becomes much larger than the coarse simulations with values reaching above 120 m s^{-1} at 3.5 h for short time intervals. This result is similar to that documented in Rotunno et al. (2009) using the WRF ARW model. When examining the maximum azimuthally averaged wind speed (Fig. 8b), the large fluctuations in values are removed but the mean vortex intensity is still higher in the LES by up to ~ 30 % at 3.5 h.

Figures highlighting the radius-height structure of the primary and secondary circulations of the simulations as well as the individual terms in (5) have been produced and analyzed. For brevity, only those figures that provide insight into the role of asymmetric dynamics are presented and discussed here. Figure 9 shows the net time tendency term [LHS of (5)], net symmetric flux convergence term [sum of first two terms on RHS of (5)], net asymmetric flux convergence term [sum of third and fourth terms on RHS of (5)] and sub-grid scale diffusion term [last term on RHS of (5)] averaged over height (0 – 3 km) and time (2.5 – 3.5 h). This time period was chosen due to the significant intensification occurring in the storm (Figs. 8a and 8b) and the height interval was chosen to focus on the low-level dynamics. The coarse simulation with larger diffusion coefficients (Fig. 9a) shows that the time tendency is dominated by the sub-grid scale diffusion with large increases radially inward of ~ 15 km. The net symmetric term also contributes substantially to the time tendency as a result of the heat forcing with peak values slightly inside the RMW at ~ 18 km. The net asymmetric term is slightly negative at most radii and doesn't make much of a contribution to the time tendency. From a physics point of view, the symmetric response to the heating is intensifying and contracting the hurricane, while diffusion is mixing/smoothing the large gradients in AAM, which moves momentum in the downgradient direction (from the eyewall to the eye).

The net symmetric and asymmetric terms for the coarse simulation with lower diffusion (Fig. 9b) shows similar results to the higher diffusion simulation (Fig. 9a) although the net asymmetric term is slightly larger. As expected, the sub-grid diffusion term in Fig. 9b is very small and plays no real role in the AAM evolution. As a result, the vast majority of the intensification signal seen through the time tendency term is controlled by the symmetric response to the heating with some reduction in AAM from the net asymmetric term around the RMW. The vortex in the low diffusion run becomes a bit more intense than the high diffusion run because the downgradient movement of AAM spins down the bulk of the eyewall (located at and inside the RMW), which is negligible in the low diffusion simulation. This explanation is consistent with the findings of Bryan and Rotunno (2009) as they showed that stronger diffusion reduces the radial gradients of momentum, which leads to a weaker storm due to thermal wind balance considerations.

In the LES, the net asymmetric term (Fig. 9c) plays a major role in the AAM time tendency with values similar to or larger than the net symmetric term, which is in stark contrast to both coarse simulations. The net asymmetric term has a significant spin-down signal from a radius of ~ 15 – 30 km peaking near the RMW and a strong spin-up signal radially inside ~ 15 km. The resolved turbulence leads to enhanced eddy fluxes of AAM from the eyewall to the eye, which spins up the eye circulation. In addition, a portion of these eddy fluxes are expected to contract the mean eyewall and amplify the tangential flow through conservation of AAM arguments. Animations of the wind field indicate that the turbulent eddies are forming at the eye-eyewall interface where strong radial shear of the tangential flow is found. Emanuel et al. (1997) and earlier papers such as Smith (1980) showed through theoretical arguments that the mechanical spin-up of the eye by radial turbulent fluxes of AAM from the eyewall is important for accelerated intensification of hurricanes. The spin-up of the eye is related to the breakdown of the strong eyewall gradients and requires an increase of the warm core (via subsidence) of the storm to maintain thermal wind balance.

Is the standard downgradient diffusion [Laplacian operator in (3) and (6)] used to model the effects of sub-grid turbulence in the coarse simulation a good approximation of the LES? While the overall trend of spreading AAM from the eyewall to the eye is captured by the Laplacian diffusion, it is clear that complicated, small-scale details in the LES can have important consequences for the mean hurricane. After all, the azimuthal mean wind speed is up to ~ 30 % stronger in the LES for short time integrations of 3.5 h (Fig. 8b). Note that the time tendency of AAM is negative from ~ 18 – 25 km radius in the coarse simulation with large diffusion (Fig. 9a) and positive in the same region in the LES (Fig. 9c), which could explain some of the differences in mean intensity. A flow dependent eddy viscosity should improve the modeling of the LES effects. However, the first order turbulence closure assumes that the AAM transport is purely downgradient, which may not be the case in the LES. For example, eye-eyewall interaction facilitated by mesovortices can transport momentum upgradient and can be regarded as a non-local, advective process, requiring more advanced turbulence modeling in the coarse simulation.

The net symmetric term has similar structure and magnitudes to the coarse simulations (especially the low diffusion run) in the main portion of the eyewall. However, in the eye region centered at ~ 10 km radius there is a mean spin-down effect, which is not observed in either coarse simulation. The main focus in this section is the role of the asymmetric dynamics so the details of this feature are not analyzed here.

Figure 10 shows the AAM budget terms averaged over height (3 – 6 km) and time (2.5 – 3.5 h) to highlight the dynamics in the mid-levels of the hurricane. The net symmetric and diffusion terms in all simulations have similar resemblance to their low-level counterparts (Fig. 9) with the exception of a symmetric spin-down effect in the eye of the vortex (radius ~ 10 km) for both coarse simulations (Figs. 10a and 10b). The net asymmetric term in both coarse simulations plays a larger role in the AAM time tendency than at low-levels, which may be due to stronger vorticity generation in this layer as the peak in heating tends to maximize around 5 km height. In all simulations, the asymmetric term is responsible for a spin-down of the main portion of the eyewall centered at the RMW and a spin-up effect radially inside of ~ 15 km radius, which is similar to that observed at low-levels in the LES (Fig. 9c).

Note that the coarse simulation with large diffusion (Fig. 10a) shows a negative AAM time tendency in portions of the eyewall (radius of ~ 20 – 30 km), which is not observed in the LES (Fig. 10c). *The negative tendency is due to the combined effects of diffusion and the asymmetric term, which indicates that the sub-grid diffusion is overly dissipative when compared to a simulation where those eddies are resolved.* Of course, we are using constant diffusion coefficients, which is not the best assumption, but many studies use this simple sub-grid model at coarse resolutions to understand the basic impacts of symmetric and asymmetric dynamics in hurricanes (e.g. Nolan and Grasso 2003).

5. CONCLUSIONS

Recent studies of hurricanes have focused on the importance of turbulence in intensity change, especially in the boundary layer. In this paper, a LES (60 m grid spacing) of an intensifying hurricane modeled after Hurricane Guillermo (1997) was conducted to provide data for the design of radar instrumentation and retrieval algorithms in addition to understanding the role of asymmetric dynamics. Comparisons of the LES to flight level data in Guillermo showed a reasonable agreement in terms of statistical properties of turbulence such as the distribution and spectral characteristics of turbulent kinetic energy. Simulated conically scanning airborne radar measurements and 3D wind vector retrievals modeled after the IWRAP instrument are able to fully resolve scales on the order of ~ 1 km, which is a typical scale for large turbulent eddies in hurricanes. This scale is responsible for most of the energy production and transport of quantities to other regions of the hurricane, such as fluxes of momentum out of the boundary layer and into the bulk vortex.

Angular momentum budgets showed a substantial spin-up signal from purely asymmetric processes during the intensification of the Guillermo-like simulation at 60 m resolution. Identical simulations at 2 km resolution do not show this asymmetric spin-up signal at low-levels (0 – 3 km layer), which is consistent with a weaker mean vortex in the coarse run. The breakdown of the strong shear at the eye-eyewall interface into turbulent eddies in the 60 m simulation is a primary reason for this enhanced eddy momentum flux signal. This added torque to the eye allows subsidence warming to occur in order to maintain thermal wind balance (Smith et al. 1980; Emanuel 1997). The present work is preliminary and more analysis and simulation sensitivity tests are needed to understand and extend these potentially important results.

Acknowledgements. Steve Guimond was partially supported by the NASA EPOCH mission for a portion of this study. Sydney Sroka was supported by a NASA internship during the summer of 2017 and Devin Protzko was supported by a SURE award to Steve Guimond at UMBC.

REFERENCES

Bryan, G. H., and R. Rotunno, 2009: The maximum intensity of tropical cyclones in axisymmetric numerical model simulations. *Mon. Wea. Rev.,* **137,** 1770–1789.

Bryan, G.H., Rotunno, R., and Y. Chen, 2010: The effects of turbulence on hurricane intensity. *29th Conference on Hurricanes and Tropical Meteorology,* Amer. Meteor. Soc., Tucson, AZ, 8C.7.

Emanuel, K.A., 1986: An air-sea interaction theory for tropical cyclones. Part I: Steady-state maintenance. *J. Atmos. Sci.*, **43,** 2044-2061.

Emanuel, K.A., 1997: Some aspects of hurricane inner-core dynamics and energetics. *J. Atmos. Sci.*, **54,** 1014 – 1026.

Fernandez, D., E. A. Kerr, A. Castells, S. J. Frasier, J. R. Carswell, P. S. Chang, P. Black, and F. D. Marks, 2005: IWRAP: The imaging wind and rain airborne profiler for remote sensing of the ocean and the atmospheric boundary layer within tropical cyclones, *IEEE Trans. Geosci. Remote Sensing,* **43(8),** doi:10.1109/TGRS.2005.851,640.

Grinstein, F.F., L.G. Margolin and W.J. Rider, 2007: *Implicit Large Eddy Simulation: Computing Turbulent Fluid Dynamics*. Cambridge University Press, 577 pp.

Guimond, S.R., M.A. Bourassa, and P.D. Reasor, 2011: A latent heat retrieval and its effects on the intensity and structure change of Hurricane Guillermo (1997). Part I: The algorithm and observations. *J. Atmos. Sci.*, **68,** 1549-1567.

Guimond, S.R., and J.M. Reisner, 2012: A latent heat retrieval and its effects on the intensity and structure change of Hurricane Guillermo (1997). Part II: Numerical simulations. *J. Atmos. Sci.*, **69,** 3128-3146.

Guimond, S.R., L. Tian, G.M. Heymsfield and S.J. Frasier, 2014: Wind retrieval algorithms for the IWRAP and HIWRAP airborne Doppler radars with applications to hurricanes. *J. Atmos. Oceanic Technol.,* **31,** 1189 – 1215.

Guimond, S.R., J.M. Reisner, S.M. Marras and F.X. Giraldo, 2016: The impacts of dry dynamic cores on asymmetric hurricane intensification. *J. Atmos. Sci.*, **73,** 4661 – 4684.

Guimond, S.R., J.A. Zhang, J. Sapp, and S.J. Frasier, 2018: Coherent turbulence in the boundary layer of Hurricane Rita (2005) during an eyewall replacement cycle. *J. Atmos. Sci.*, accepted pending revision.

Montgomery, M. T., M. Nicholls, T. Cram, and A. Saunders, 2006: A vortical hot tower route to tropical cyclogenesis. *J. Atmos. Sci.*, **63**, 355–386.

Nakanishi, M., and H. Niino, 2012: Large-eddy simulation of roll vortices in a hurricane boundary layer. *J. Atmos. Sci.*, **69,** 3558 – 3575.

Nolan, D.S., and L.D. Grasso, 2003: Nonhydrostatic, three-dimensional perturbations to balanced, hurricane-like vortices. Part II: Symmetric response and nonlinear simulations. *J. Atmos. Sci.*, **60,** 2717-2745.

Persing, J., M.T. Montgomery, J.C. McWilliams, R.K. Smith, 2013: Asymmetric and axisymmetric dynamics of tropical cyclones. *Atmos. Chem. Phys.*, **13,** 12299 – 12341.

Reisner, J. M., V. A. Mousseau, A. A. Wyszogrodzki, and D. A. Knoll, 2005: An implicitly balanced hurricane model with physics-based preconditioning. *Mon. Wea. Rev.*, **133**, 1003–1022.

Rotunno, R., Y. Chen, W. Wang, C. Davis, J.Dudhia, and G.J. Holland, 2009: Large-eddy simulation of an idealized tropical cyclone. *Bull. Amer. Meteor. Soc.*, **90,** 1783 – 1788.

Smith, R.K., 1980: Tropical cyclone eye dynamics. *J. Atmos. Sci.*, **37,** 1227 – 1232.

Stull, R.B., 1988: *An Introduction to Boundary Layer Meteorology*. Kluwer Academic Publishers, 666 pp.

Tennekes, H., and J.L. Lumley, 1972: *A First Course in Turbulence*. M.I.T. Press, 300pp.

Zhang, J.A., W.M. Drennan, P.G. Black and J.R. French, 2009: Turbulence structure of the hurricane boundary layer between the outer rainbands. *J. Atmos. Sci.*, **66,** 2455 – 2467.

Zhang, J. A., F. D. Marks, M. T. Montgomery, and S. Lorsolo, 2011: An estimation of turbulent characteristics in the low-level region of intense Hurricanes Allen (1980) and Hugo (1989). *Mon. Wea. Rev*., **139**, 1447–1462.

Figures

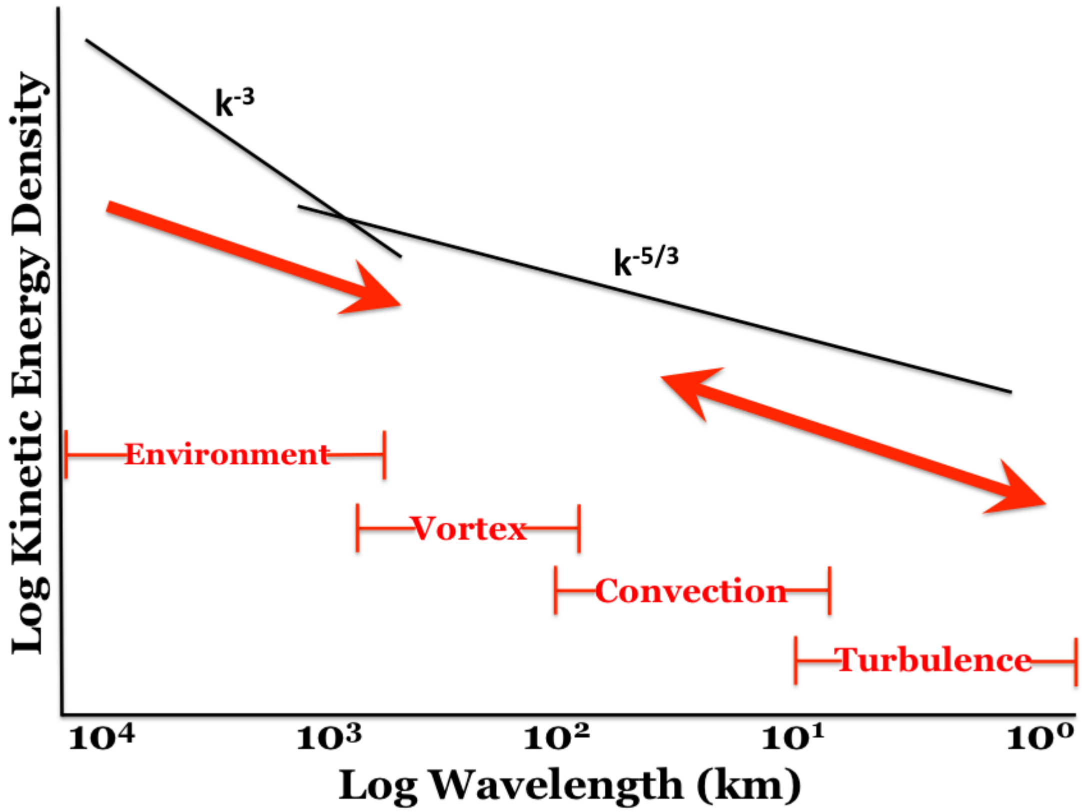

Figure 1. Schematic of the kinetic energy density as a function of wavelength for the physical processes controlling the intensification of hurricanes. Black lines highlight the expected energy scaling from turbulence theory and red arrows denote the direction of nonlinear energy transfer.

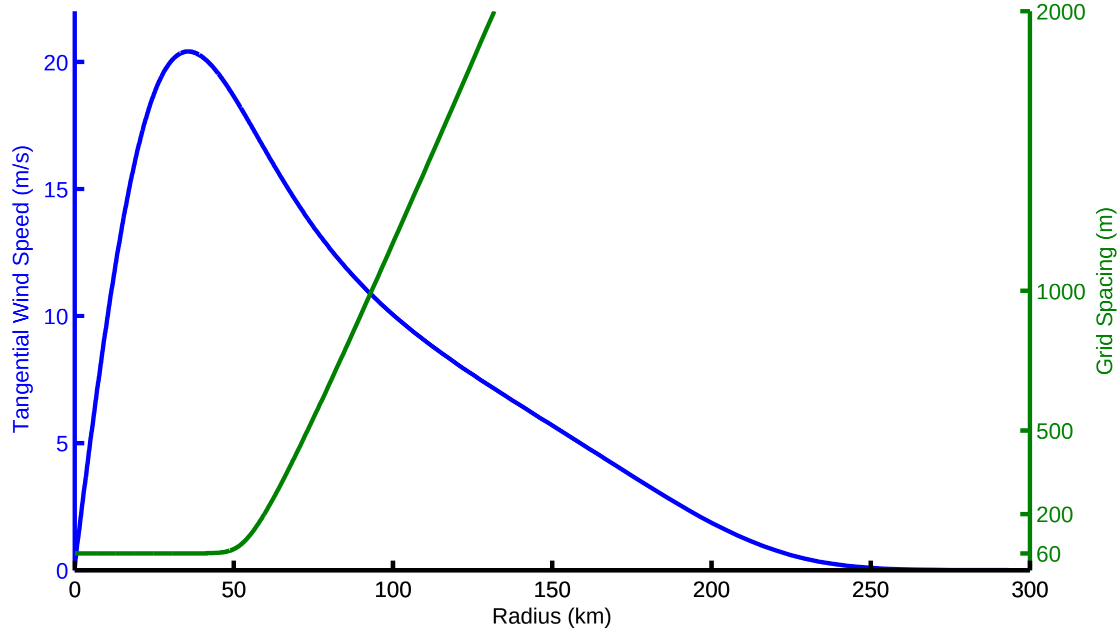

Figure 2. Radial profile of the initial, balanced tangential wind at the lowest model level along with the associated grid spacing of the mesh.

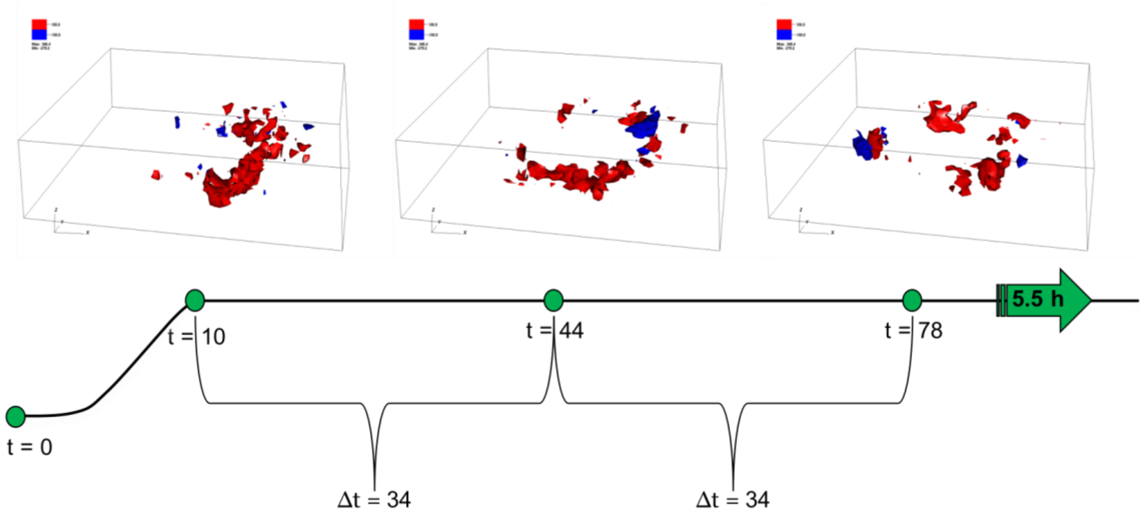

Figure 3. Three-dimensional isosurfaces of the latent heating (red contours; 100 K h^{-1}) and cooling (blue contours; -100 K h^{-1}) retrievals in Hurricane Guillermo (1997) for three example time periods. Each box is centered on the storm with a length of 120 km in the horizontal dimensions and 20 km in the vertical dimension. The data are introduced into the model using a time evolution function visualized in the figure. Details can be found in Guimond et al. (2012).

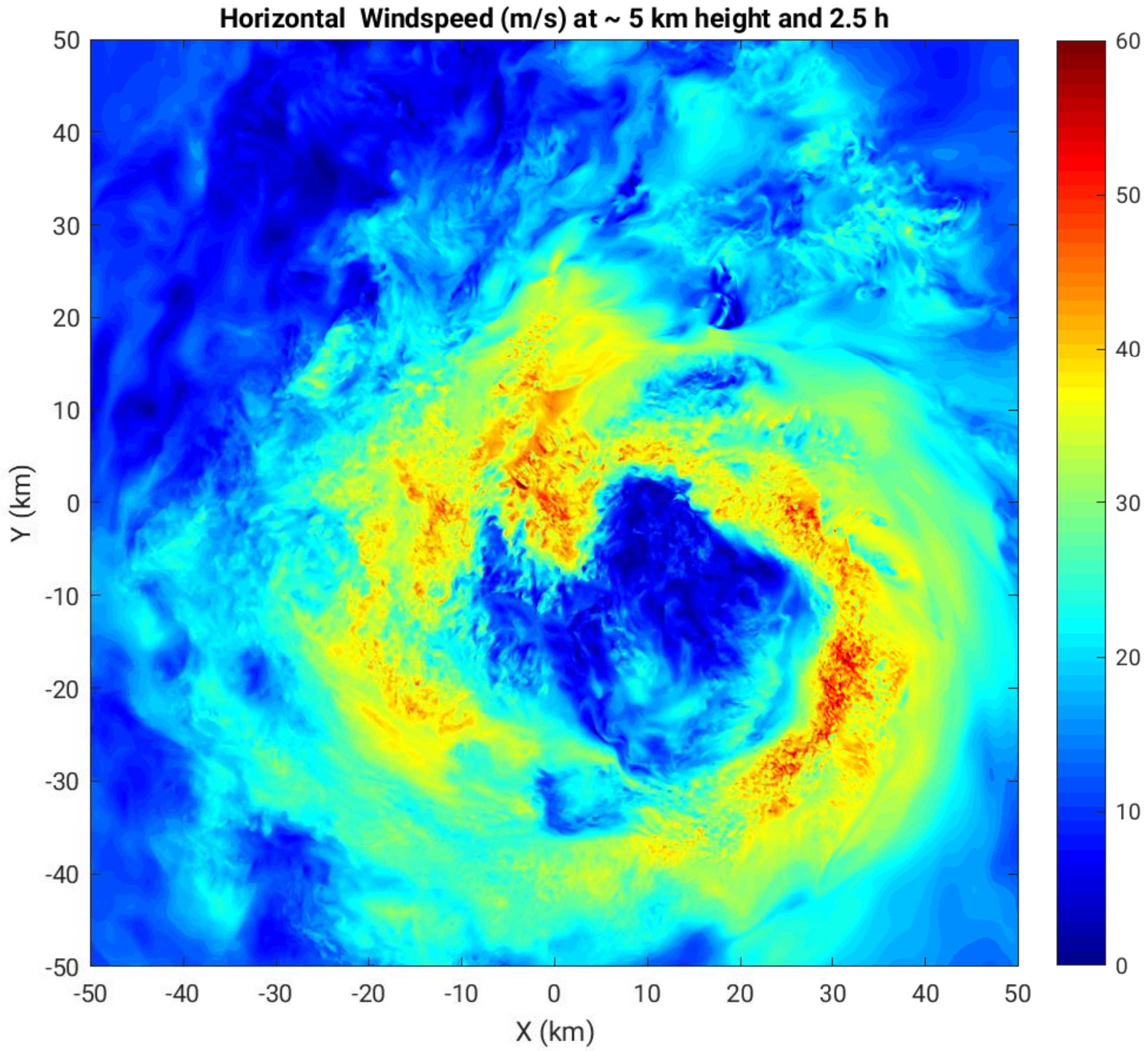

Figure 4. Horizontal windspeed at 5 km height and 2.5 h into the LES showing the inner 100 km^2 area of the model domain.

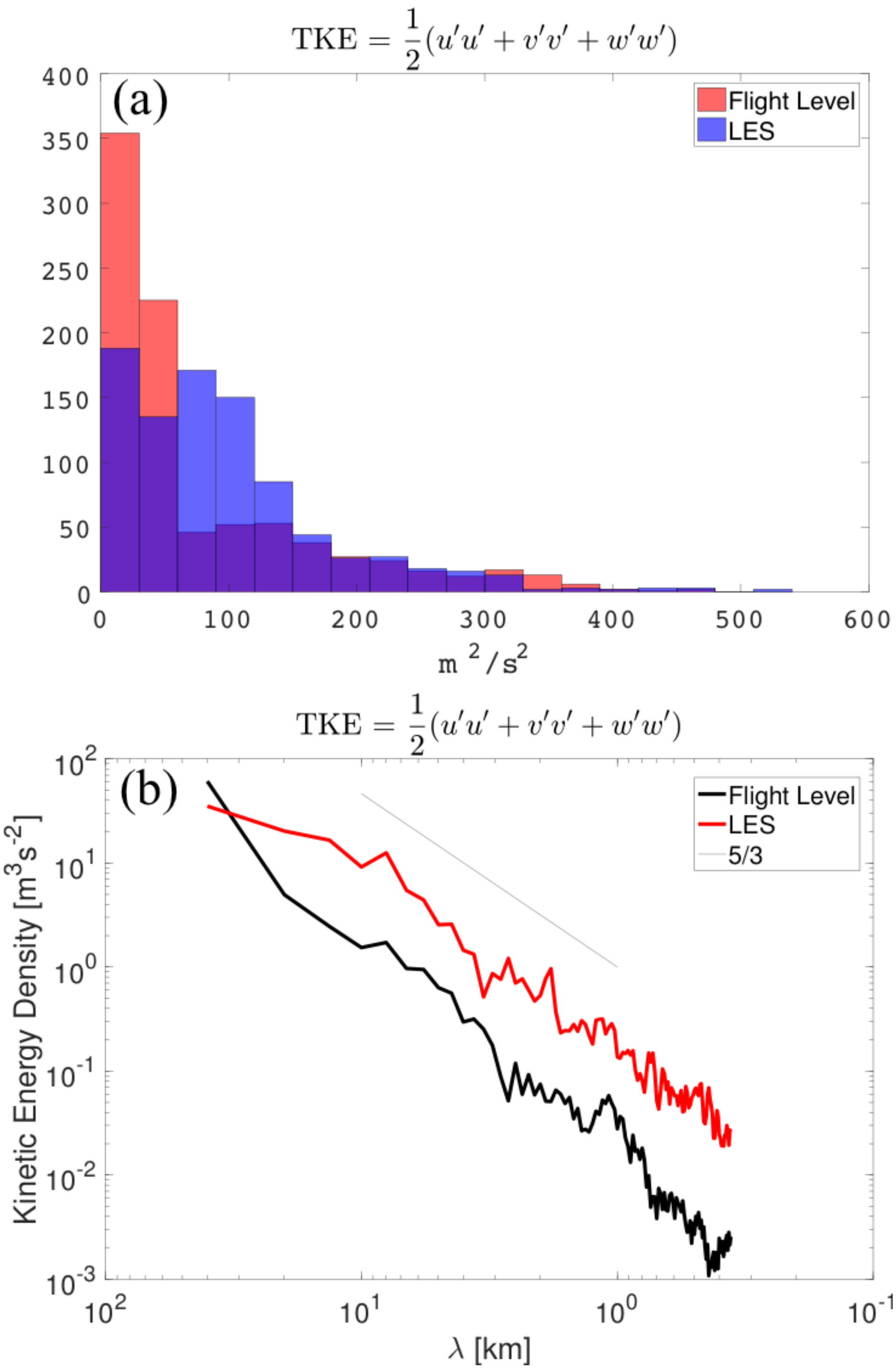

Figure 5. Comparisons of turbulence statistics between flight level observations in Hurricane Guillermo (1997) and the LES for (a) histograms of the turbulent kinetic energy and (b) mean spectrum of the turbulent kinetic energy as a function of wavelength. See text for details.

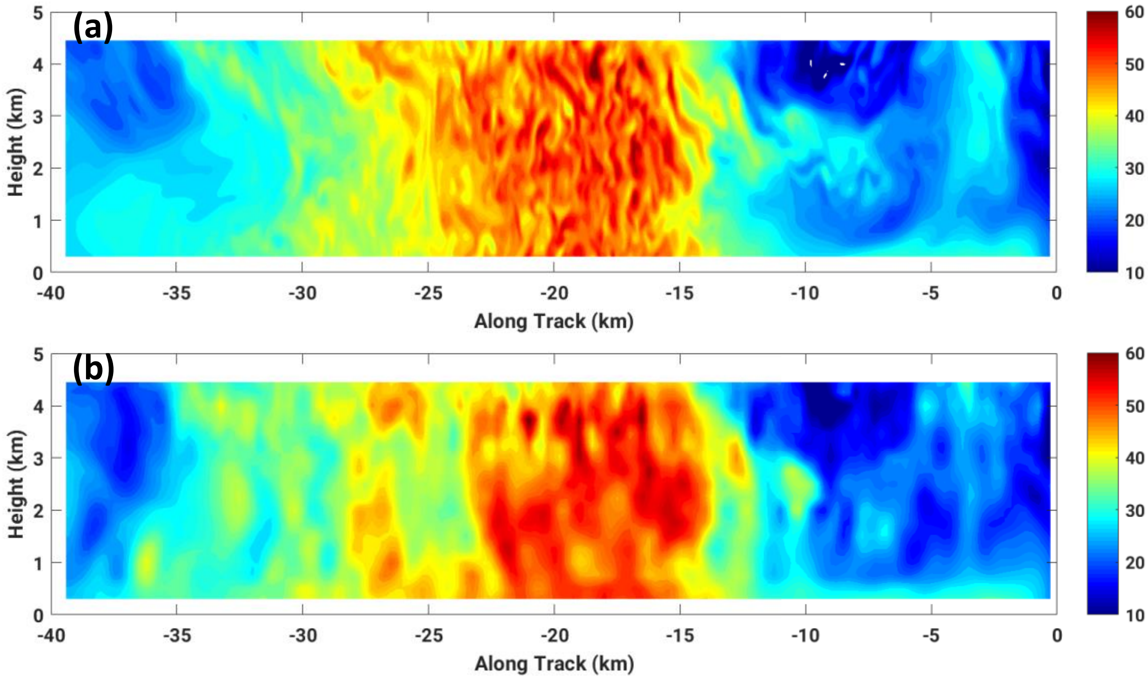

Figure 6. Nadir vertical cross sections of horizontal wind speed through the simulated radar sampling volume for a typical radial flight leg of IWRAP data. The panels show (a) the simulated truth field from the LES and (b) the retrieved field using IWRAP specifications.

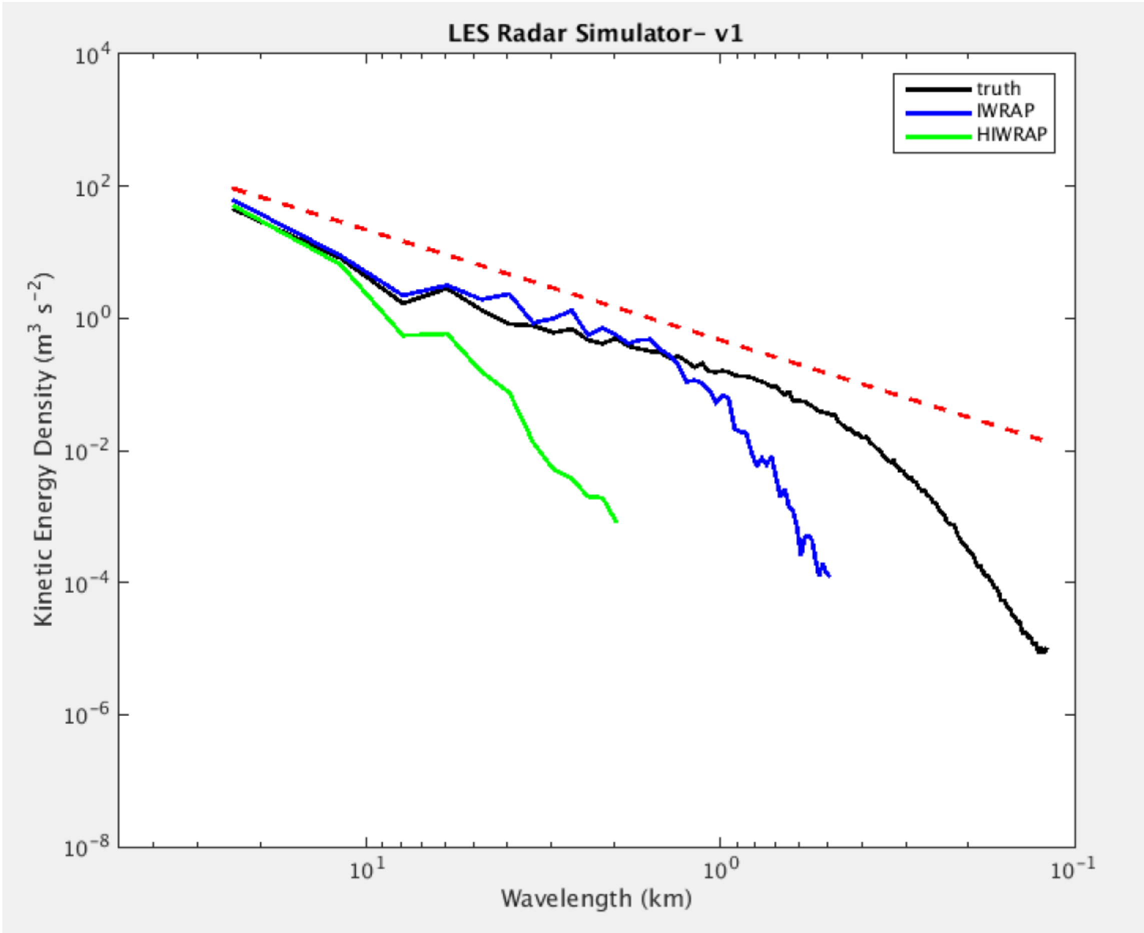

Figure 7. Comparison of the kinetic energy spectrum averaged over the radar sampling volume for the numerically simulated truth (black line) and the IWRAP wind retrievals (blue line). The green line shows preliminary results for a slower scanning radar at 16 RPM. The red dashed line is the -5/3 energy slope from turbulence theory.

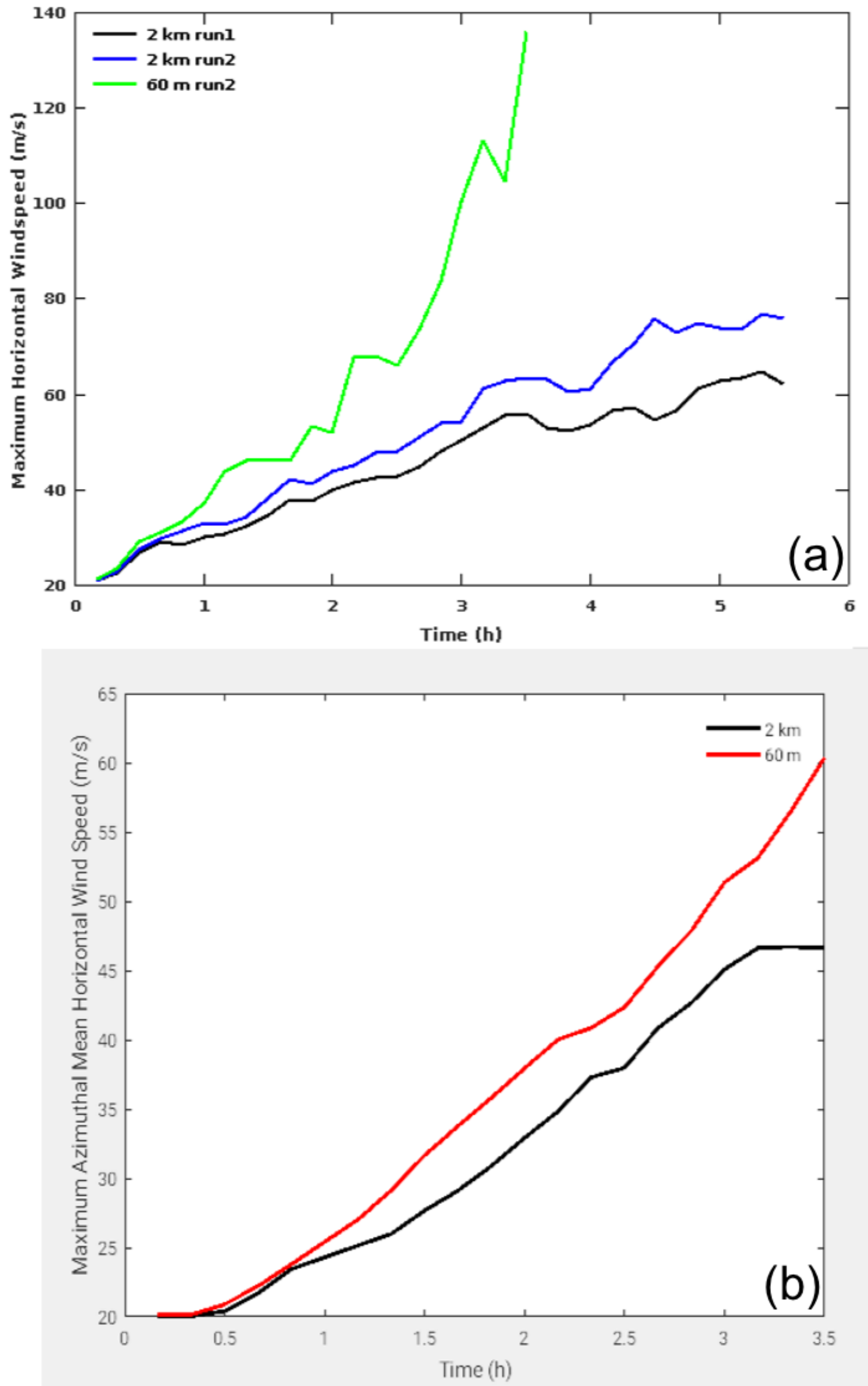

Figure 8. Time series of (a) maximum horizontal windspeed for the LES (green line), coarse simulation with the same diffusion coefficients as the LES (blue line), coarse simulation with κ_h = 20,000 m^2 s^{-1} and κ_v = 400 m^2 s^{-1} (black line) and (b) maximum azimuthally averaged horizontal wind speed for the LES (red line) and the coarse simulation with κ_h = 20,000 m^2 s^{-1} and κ_v = 400 m^2 s^{-1}.

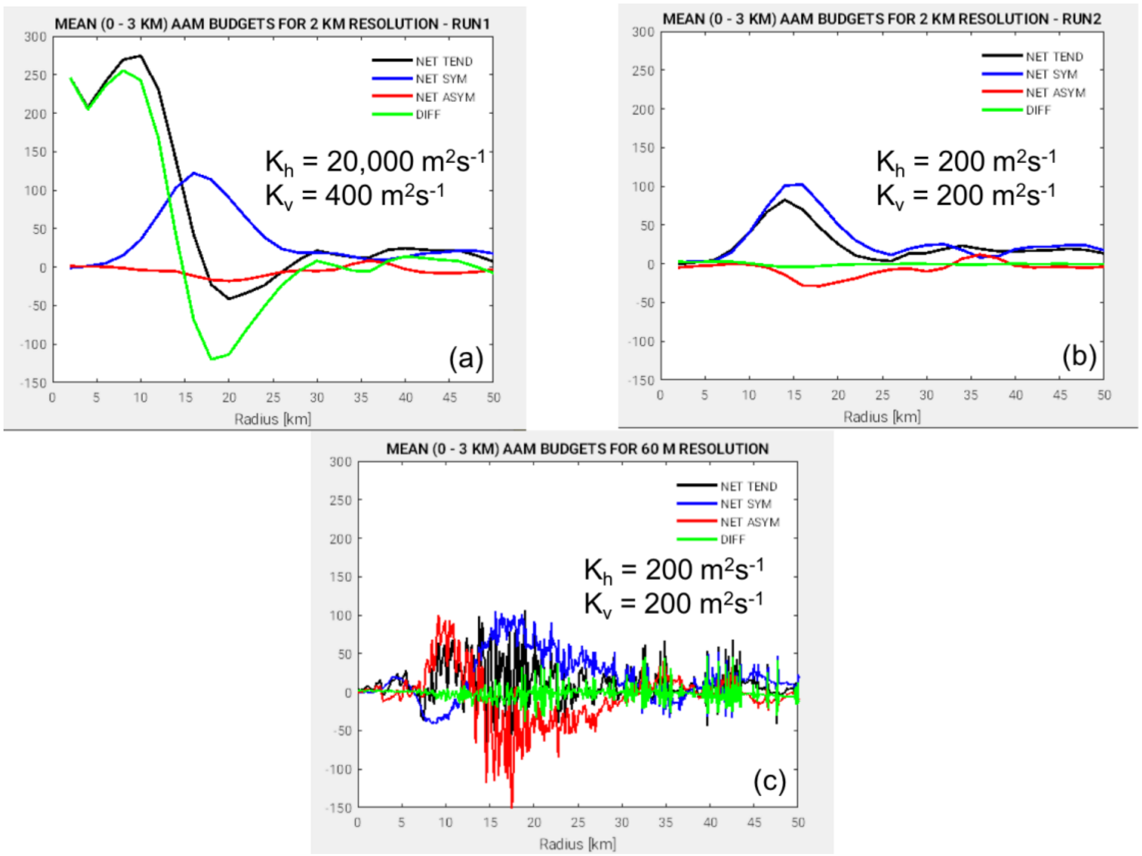

Figure 9. Absolute angular momentum budgets for (a) the 2 km simulation with eddy diffusion coefficients scaled to compare with the LES, (b) the 2 km simulation with the same eddy diffusion coefficients as the LES and (c) the LES. Terms in the budget are averaged over height (0 – 3 km) and time (2.5 – 3.5 h).

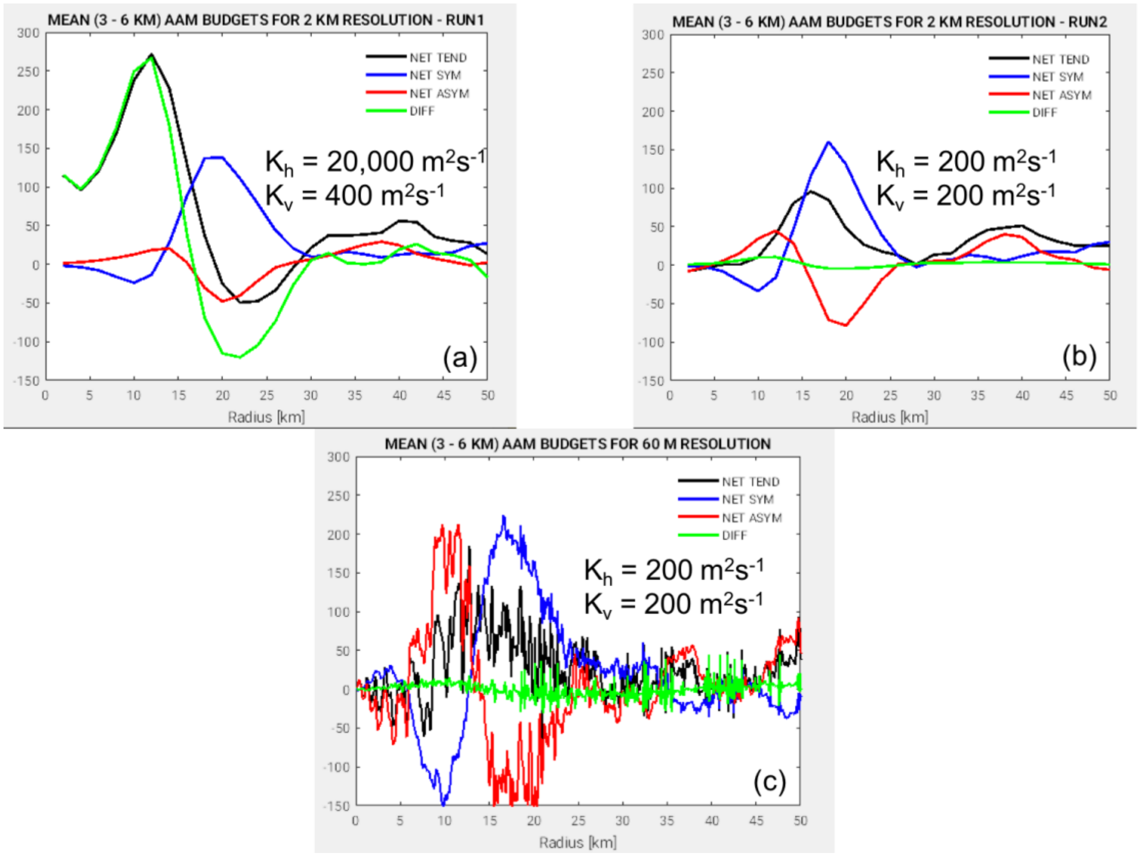

Figure 10. The same as in Fig. 9, only averaged over the 3 – 6 km layer.